

Article

High-Temperature and High-Pressure Tribological Properties of Siliconized Graphite for Water-Lubricated Thrust Bearing Application in Main Coolant Pump

Sihang Liu ¹, Baojun Zhang ^{1,2}, Long Cai ^{1,3}, Weiguang Wang ^{1,3}, Taihe Liang ¹ and Mingkai Lei ^{1,*}

¹ Surface Engineering Laboratory, School of Materials Science and Engineering, Dalian University of Technology, Dalian 116024, China; shliu@mail.dlut.edu.cn (S.L.); baojun_z@mail.dlut.edu.cn (B.Z.); hpc_cailong@harbin-electric.com (L.C.); hpc_wangweiguang@harbin-electric.com (W.W.); thliang@mail.dlut.edu.cn (T.L.)

² Sinoseal Holding Co., Ltd., Chengdu 610045, China

³ Harbin Electric Power Equipment Co., Ltd., Harbin 150040, China

* Correspondence: surfeng@dlut.edu.cn

Abstract: The effect of the microstructure of siliconized graphite on tribological properties is investigated by using a high-temperature and high-pressure water-lubricated tribometer on a self-mated ring-on-ring configuration under an applied load of 500–1500 N with a spindle speed of 100–5000 rpm in both 90 °C (5 MPa) and 25 °C (1 MPa) water environments, respectively. The Stribeck curves measurement and continuous wear tests are performed and analyzed in both water environments. The wear behaviors of the graphite, SiC, and free-silicon phases in siliconized graphite are demonstrated to explore the wear mechanism. The larger wear depths of a low-worn surface roughness on the three phases contribute to the boundary lubrication. The shallower wear depths are observed on the SiC and Si phases under the mixed lubrication, corresponding to partial contact wear of surface asperities. The wavy surface of the SiC phase and uniform flow-oriented striae of the Si phase are attributed to hydrodynamic lubrication, caused by full water film scouring the worn surface. Finally, an integrated evaluation method of *G* duty parameters is successfully used to identify the lubrication regimes of siliconized graphite from the boundary, mixed, to hydrodynamic lubrications for a water-lubricated thrust bearing application in the main coolant pump of a nuclear power plant.

Keywords: siliconized graphite; high-temperature and high-pressure water; lubrication regime; wear mechanism; Stribeck curve; *G* duty parameters



Citation: Liu, S.; Zhang, B.; Cai, L.; Wang, W.; Liang, T.; Lei, M. High-Temperature and High-Pressure Tribological Properties of Siliconized Graphite for Water-Lubricated Thrust Bearing Application in Main Coolant Pump. *Lubricants* **2024**, *12*, 159.

<https://doi.org/10.3390/lubricants12050159>

Received: 8 April 2024

Revised: 16 April 2024

Accepted: 1 May 2024

Published: 3 May 2024



Copyright: © 2024 by the authors. Licensee MDPI, Basel, Switzerland. This article is an open access article distributed under the terms and conditions of the Creative Commons Attribution (CC BY) license (<https://creativecommons.org/licenses/by/4.0/>).

1. Introduction

The water-lubricated thrust bearings in the main coolant pump of a nuclear power plant operate in the coolant of various temperatures and pressures under different lubrication regimes are subjected to extremely high load, high rotation speed, and frequent startup and shutdown conditions [1–3], etc. As a core component of the main coolant pump, its friction stability with low wear loss is crucial to the safe and long-term operation of a primary coolant loop. The service life and tribological properties of thrust bearings mainly depend on the friction pair material and operating conditions. Yu et al. [4] reported that the applied load is the main fact affecting lubrication film pressure and the rotational speed has a significant impact on the film temperature with a matching relationship between the load and rotational speed. Huang et al. [5] found that the temperature-induced deformation of friction pairs in water results in aggravated friction and wear for the polymer resin materials when the temperature exceeds 80 °C. Kitaoka et al. [6] conducted a comparison of tribological behaviors of self-mated SiC ceramics experiencing a sliding motion in different temperature and pressure water environments. The wear mechanism of SiC in the water is tribochemical wear, because the hydrothermal oxidation of SiC increases with the

temperature. Yin et al. [7] observed that the direct contact of friction pairs vastly increases with speed due to the thermal compression and accumulation effect at the low initial temperature. The friction pair materials of water-lubricated thrust bearings have a significant effect on lubrication regimes from the hydrodynamic one to the mixed lubrication one and, degeneratively, to the wear regime.

Siliconized graphite is primarily used for water-lubricated thrust bearings in the high-loading systems of a primary coolant loop under a loading pressure of up to 0.8 MPa at a water temperature of 70–90 °C [8,9]. Compared with the thrust bearing materials of polymers [10,11], composites [12,13], and ceramics [14,15], etc., the tribological behaviors of siliconized graphite under water lubrication is more complex, due to its multi-phase structure and microstructure. Xia et al. [16] found that the ploughing wear of siliconized graphite is mainly a dry wear mechanism coupled with abrasive and adhesive wear, resulting in a lower wear rate but in a higher coefficient of friction (COF). Subsequently, Xue et al. [17] observed the abrasive wear mechanism of siliconized graphite under boundary lubrication in ambient water. Li et al. [18] compared the two tribological types of siliconized graphite in ambient water and pointed out the content ratio leading to the different wear mechanisms. Yuan et al. [19] found that water lubrication decreases the friction and wear of SiC mainly by the formation of a SiO₂ tribo-layer, whereas the graphene lubricant reduces the COF. However, the literature available pertaining to the tribological properties of siliconized graphite in high-temperature and high-pressure water environments for water-lubricated thrust bearing applications is limited. Particularly, the lubrication regime of siliconized graphite needs to be systematically investigated under the startup and shutdown and even extreme operating conditions usually serve in the thrust bearings of the main coolant pump.

In this article, the effect of the microstructure of siliconized graphite on tribological properties is investigated by using a high-temperature and high-pressure water-lubricated tribometer on a self-mated ring-on-ring configuration. Spindle speeds of 100–5000 rpm under the loads of 500–1500 N are implemented in both 90 °C (5 MPa) and 25 °C (1 MPa) pure water environments. The Stribeck curves are measured as the COF values of siliconized graphite rings as a function of spindle speeds during a time period of 600 s under the applied loads. In order to explore the wear mechanisms, the COF pattern, worn surface morphology, and wear depth are analyzed by special wear experiments at a continuous 7200 s duration with the selected spindle speeds under the correspondent loads in the water environments. The wear behavior of the graphite, SiC, and free-silicon phases in the siliconized graphite is demonstrated to explore the lubrication regimes of siliconized graphite. An integrated evaluation method of *G* duty parameters is proposed to identify the boundary, mixed, and hydrodynamic lubrication transition for the water-lubricated thrust bearings of the main coolant pump in a nuclear power plant.

2. Experimental

2.1. Tribological Experiment in High-Temperature and High-Pressure Water

A modified high-temperature and high-pressure water tribometer is used to investigate the tribological properties in different temperature and pressure water environments. Figure 1 shows the schematic diagram of the high-temperature and high-pressure water tribometer. The ring-on-ring (disc-to-disc) and pin-on-disc configurations of self-leveling devices are, respectively, implemented to ensure full-pair contact under the maximal applied load of 2000 N from the pneumatic loading device, which can simulate a contact pressure of nearly 0.01–4.00 MPa. The maximal water temperature of the tribometer can be adjusted up to 300 °C at the maximal water pressure of 10 MPa by the electric heater. Servo high-speed motor power of 40 kW provides a spindle speed up to 10⁴ rpm, which is equivalent to obtaining an average sliding speed of 50 m/s. The motor drives the spindle to rotate the top specimen ring, and the static bottom specimen ring is lifted by the axial loading of the pneumatic cylinder through the shaft, which is controlled by a force sensor. The non-contact sensors measure and collect friction torque/force data, and the displacement sensors are used for in situ wear depth measurement. All parameters are observed in real

time. The no-load torque is initially calibrated with each speed involved in the experiment in the water environment. The friction force is then calculated by subtracting the no-load torque to eliminate the additional torque from other rotating components, such as bearing parts with seal. The computer software with logic control may continuously control all the settings of water temperature and pressure, as well as load and speed parameters. Key components and layout of the modified tribometer are broadly outlined (Figure 1a). In addition to the main part, the tribometer comprises other auxiliary systems like supply gas source, oil station, and water station.

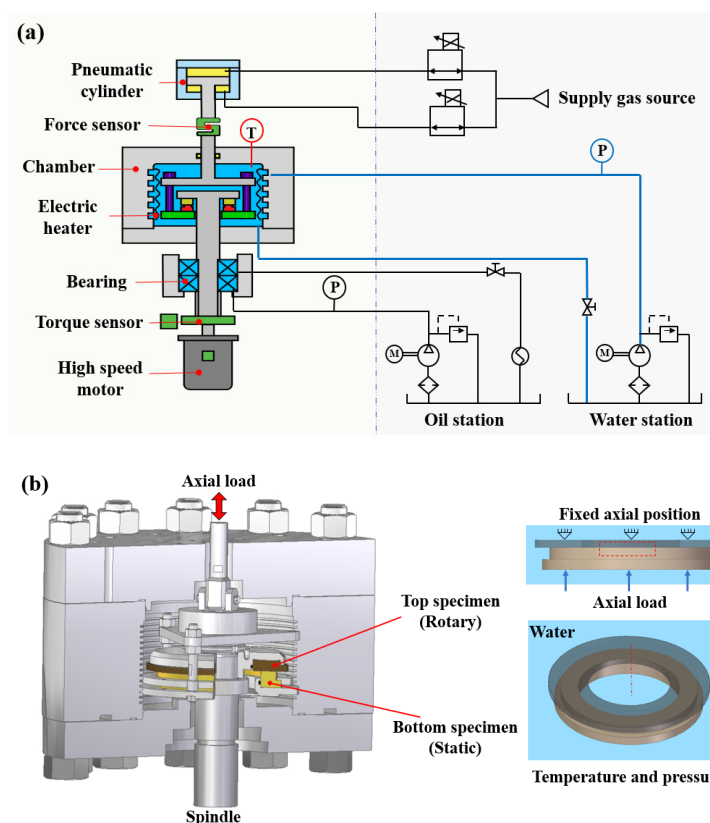


Figure 1. Schematic diagram of the high-temperature and high-pressure water-lubricated tribometer. (a) Overall and (b) assembly in chamber.

In this work, the system used a ring-on-ring configuration, exposing the friction pairs to sliding conditions at high velocities, high-contact pressure, and controlled environment in the high-temperature and high-pressure water (Figure 1b). The siliconized graphite was prepared by liquid silicon infiltration method in a high-temperature furnace. A round carbon preform disc was packed in a bed of Si powder inside a high-density graphite crucible with a lid. The reaction was carried out at the firing temperature of 1500 °C in a vacuum atmosphere for 1 h. After infiltration, the siliconized graphite was washed by hydrofluoric acid and then machined into friction ring. The sizes of the top and bottom rings were 67 mm and 82 mm in inner diameter, 130 mm and 110 mm in outer diameter, and 10 mm in thickness, with a total contact area of 4220.16 mm². The siliconized graphite rings were all ground and polished prior to characterization and testing, and flatness was ensured to be less than 0.9 μm.

Two types of experiments were carried out, namely (I) Stribeck curve measurements in high-temperature and high-pressure water and (II) wear tests at high-temperature and high-pressure water-lubricated condition during a long time of 7200 s. The experimental conditions are summarized in Table 1. The high-water temperature of 90 °C at the high-water pressure of 5 MPa was subjected to simulate the service environment of siliconized graphite in thrust bearings in a main coolant pump. The room temperature of 25 °C at

pressure of 1 MPa was used as a reference. The corresponding loads and speeds were implemented according to the service condition of thrust bearings. Experimental programs for (I) Stribeck curve measurements included four groups as applied loads of 500 N, 800 N, 1100 N, and 1500 N in 25 °C (1 MPa) and 90 °C (5 MPa) water, respectively. Step-down 11 speed stages were employed from 5000 rpm (which is equivalent to sliding speed of 25.0 m/s) to 100 rpm (0.5 m/s) for a stage duration of 600 s. All Stribeck curves measurements are repeated three times. Experimental programs for (II) wear tests included total of 12 sets for 7200 s in 25 °C (1 MPa) and 90 °C (5 MPa) water with corresponding load and speed. The parameter selection for the experiment (II) was based on the operating conditions corresponding to the maximal and minimal values of COF at different velocities in the Stribeck curves of the experiment (I) with the distinctly different curve feature. To more exactly measure the wear depth, three grooves of 4 × 4 mm with a depth of about 8 μm distributed on the surface of bottom ring were prepared by laser beam machining. The groove depth change was characterized as the worn depth using the average value of the trace scanned by a Surfcoorder ET4000A profilometer (Sotokanda Chiyoda-ku, Tokyo, Japan) with the tip curvature radius of 0.5 μm, scanning speed of 0.05 mm/s, and scanning distance of 4 mm. Five trace measurements were carried out on each groove, and a total of 15 values were averaged. The calculation of the in situ COF and steady-state wear depth in experiments (I) and (II) was thus enabled.

Table 1. Experimental conditions of high-temperature and high-pressure water-lubricated tribometer.

Experiment Type	Water Environment	Applied Load (N)	Speed (rpm)	Time
(I) Stribeck curves in high-temperature and high-pressure water	25 °C (1 MPa)	500	Step-down 5000–100 (25.0–0.5 m/s)	A stage duration of 600 s
		800		
		1100		
		1500		
	90 °C (5 MPa)	500		
		800		
		1100		
		1500		
(II) Wear for high-temperature and high-pressure water-lubricated tribometer	25 °C (1 MPa)	500	100	For 7200 s duration
		500	5000	
		800	1000	
		800	5000	
		1100	2000	
		1500	100	
	90 °C (5 MPa)	500	100	
		500	5000	
		800	1000	
		800	5000	
		1100	2000	
		1500	100	

2.2. Characterization of Worn Siliconized Graphite Rings

The element and phase distribution of C and Si in worn siliconized graphite rings was measured by a JXA-8530F PLUS (Akishima, Tokyo, Japan) electron probe microanalyzer (EPMA) with energy dispersive spectroscopy (EDS) detector. The worn surface morphology was also observed by scanning electron microscope (SEM). The phase content and structure of siliconized graphite was measured by a PANalytical Empyrean (Enigma Business Park, Malvern, United Kingdom) x-ray diffractometer (XRD), with CuK α radiation using a 2 θ angle ranging of 20–100°. The surface profiles of the worn siliconized graphite rings were also detected using a Surfcoorder ET4000A profilometer (Sotokanda Chiyoda-ku, Tokyo, Japan). The residual stress on the worn surface of the siliconized graphite rings was measured using the cos α method by μ -X360s's x-ray residual stress analyzer equipped with

a $\text{CrK}\alpha$ radiation. The x-ray tube voltage of 30 kV with a current of 1.5 mA, x-ray irradiation time of 15 s, and measurement time of 60 s were employed. The residual stress was analyzed from the 360° omnidirectionally diffracted sample at 125 points around Debye-Scherrer geometry. The radial residual stress around the sliding round was measured by adjusting the x-ray diffraction orientation. The graphite phases at (110) plane, Si at (331), and SiC at (222) diffraction peaks were used to characterize the residual stress, respectively. In total, 12 diffraction measurement points of the three phases were distributed on the worn ring. The nanohardness of the graphite, Si, and SiC phases were measured by NanoIndenter XPTM, MTS Systems Corporation (Eden Prairie, MN, USA) using a Berkovich diamond tip. The indentation depth was 2 μm . At least nine valid measurements were made for each phase at a separation distance of 100 μm to obtain statistical results. TEM samples of siliconized graphite ring were prepared by focused ion beam (FIB) with a FEI Helios G4 UX FIB microscope (Waltham, Massachusetts, USA). A layer of platinum was sputtered on an area of interest under electron beam condition, avoiding damage to the sputtered surface by the following gallium ion beam. The TEM samples were observed by a JEOL JEM-2100F field emission electron microscope at an accelerating voltage of 200 keV.

3. Results

3.1. Microstructure of Siliconized Graphite

Figure 2 shows the chemical composition and element distribution of the siliconized graphite. An area of $500 \times 500 \mu\text{m}$ is selected on the surface, where the distribution of C (Figure 2a) and Si (Figure 2b) is obtained. According to the gray levels of the backscattered electron diffraction image (Figure 2c), the feature extraction image is characterized as the phase distribution of siliconized graphite (Figure 2d). It is divided into three main color regions identified by the EPMA technique, namely, green for SiC, blue for graphite, and red for silicon. Photoshop software (Ps 2021) is used to identify the image and split it into 354,008 pixels. Among them, SiC is represented by green and comprises 205,798 pixels, accounting for about 58.1%; graphite by blue and is 79,333 pixels, for about 22.4%; silicon by red and is 35,710 pixels, for about 18.6%. The total recognition pixels are 350,841, and the recognition rate is 99.1%.

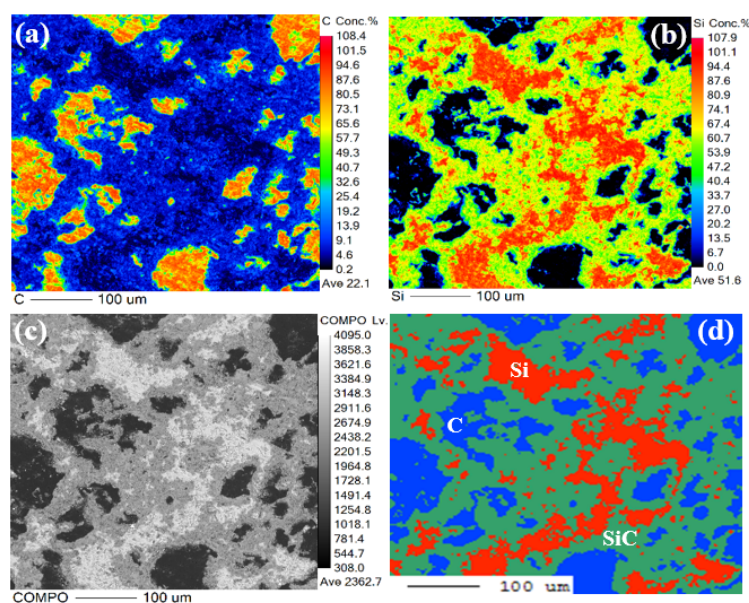


Figure 2. The chemical composition and element distribution of the siliconized graphite. (a) Distribution of C; (b) distribution of Si; (c) backscattered electron diffraction image; and (d) feature extraction image.

Figure 3 shows the XRD pattern of the siliconized graphite ring. Four main peaks of β -SiC at 2θ values of 35.6° , 41.3° , 59.9° , and 71.7° correspond to the diffraction peaks of

the (111), (200), (220), and (311) crystalline planes of the face-centered cubic lattice [20], respectively. Three main peaks of graphite-2H at 26.4° , 44.3° , and 54.5° corresponding to the diffraction of the (002), (101), and (004) planes of the hexagonal close-packed lattice [21]. Four main peaks of Si at 28.4° , 47.3° , 56.1° and 76.3° correspond to the diffraction of the (111), (220), (311), and (331) planes of the face-centered cubic lattice [22], respectively. The nanohardness of the graphite, Si, and SiC phases are measured as 0.5 ± 0.05 GPa, 12.1 ± 1.60 GPa, and 25.3 ± 3.40 GPa. The hardness gradient in the siliconized graphite leads to the complexity of the high-temperature and high-pressure water-lubricated wear.

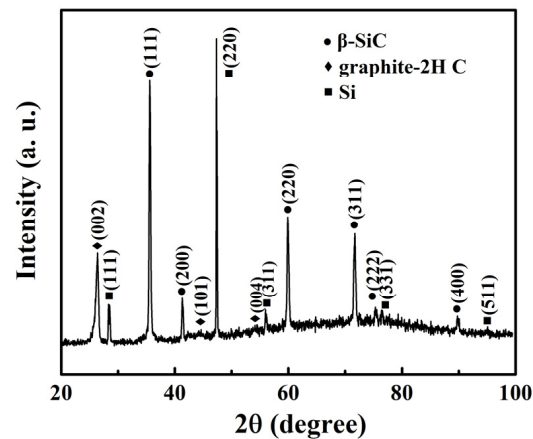


Figure 3. XRD pattern of the siliconized graphite ring.

Figure 4 shows the bright-field image of the cross-sectional transmission electron microscopy (TEM) of the siliconized graphite with the selected area electron diffraction (SAED) patterns of the Si, SiC, and graphite phases, respectively. The surface of the ground and polished siliconized graphite sample is relatively flat. There are clear interfaces among the three phases in siliconized graphite. The corresponding SAED patterns confirm that the Si and SiC phases present the face-centered cubic structures with the $\langle \bar{1}12 \rangle$ and $\langle 011 \rangle$ zone axes, respectively. The graphite has a hexagonal close-packed structure with continuously concentric diffraction rings, suggesting poor crystallinity. The formed polycrystalline structure composed of nanocrystalline graphite is attributed to the grinding process for ring preparation [23].

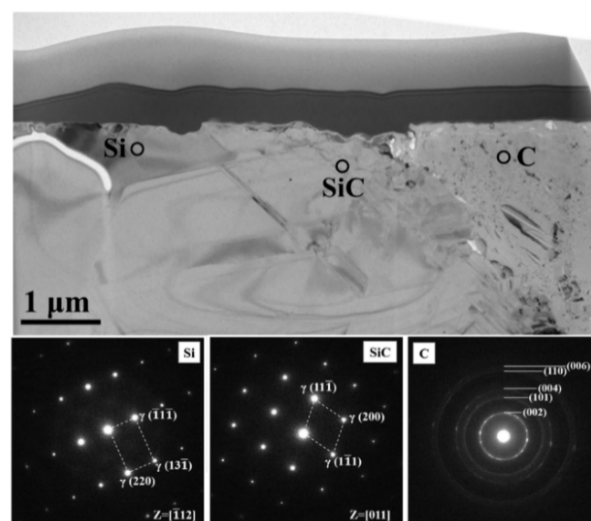


Figure 4. Bright-field image of the cross-sectional TEM sample of the siliconized graphite and SAED patterns of the Si, SiC, and graphite phases, respectively.

Therefore, siliconized graphite is prepared by the liquid silicon infiltration method with a chemical reaction of carbon and silicon, which are composed of graphite, free silicon, and β -SiC phases. Among them, SiC accounts for about 58.1%, graphite 22.4%, and silicon 18.6%. A higher development of β -SiC and a lower content of residual carbon and free silicon are observed, indicating higher reactant consumption and reaction product conversion for the materials obtained from the liquid silicon infiltration method [24,25].

3.2. Stribeck Curve Measurements

In the series of Stribeck curves measured, the spindle speed adjusts from 5000 to 100 rpm with a time duration of 600 s under the applied loads of 500–1500 N, which corresponds to a sliding speed ranging from 25.0 to 0.5 m/s. Figure 5 shows the COF values of siliconized graphite rings as a function of the step-down spindle speeds during the time stage under each load in 25 °C (1 MPa) and 90 °C (5 MPa) water environments, respectively. It is evident that the COF patterns in every time stage are fluctuated, although the fluctuation amplitudes depend on the applied loads and sliding speed during the time duration of 600 s. A distinct fluctuation peak appears in the step-down moments due to an apparent vibration with speed falling at these stages. The running-in process still exists, even in the last stabler duration of each time stage. The COF values under 500 N in 25 °C water is consistently higher with all spindle speeds, almost always exceeding 0.1. During each time stage with the higher spindle speeds of 5000–1500 rpm before 4800 s, the COF gradually increases. In contrast, the COF gradually decreases with greater fluctuation amplitude after 4800 s with the lower speeds of 1000–100 rpm. The COF under 800 N exhibits a distinct pattern, decreasing with every speed till nearly 5400 s, while the amplitude increases with speed. A lower COF value of 0.04 is achieved at 5400 s under 800 N with 1000 rpm in 25 °C water. The COF under 1100 N has a slight decrease over time, whereas that under 1500 N remains relatively stable with a value of 0.05 from the start until 4800 s and then gradually increases. The COF curve patterns in 90 °C water are similar to those in 25 °C water, but the COF values are lower under the applied loads with speed. The only difference occurs under 1100 N, where COF shows a clear trend of decreasing firstly and then increasing after 5400 s. A lower COF value is obtained as 0.03 at 5400 s under 1100 N with 1000 rpm.

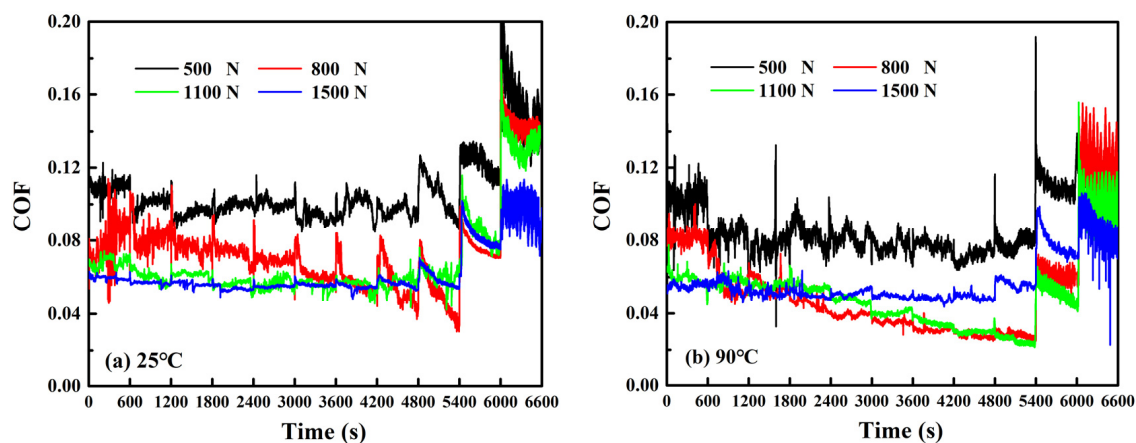


Figure 5. COF values of the siliconized graphite rings as a function of the step-down spindle speeds of 5000 rpm to 100 rpm during the time period of 600 s under applied load of 500–1500 N in (a) 25 °C (1 MPa) and (b) 90 °C (5 MPa) water environments, respectively.

Figure 6 shows the Stribeck curves of siliconized graphite rings as a function of spindle speeds from 5000 to 100 rpm under the applied loads of 500–1500 N in 25 °C and 90 °C water environments, respectively. The Stribeck curves are constructed based on the average COF value of the experimental data from Figure 5a,b. The average values are obtained for the last 300 s in the time stage of 600 s, considering the stabler COF values. For the Stribeck

curves in 25 °C water, the COF values are higher at the lower spindle speed of 100 rpm under all loads. Subsequently, there is a trend for the COF to decrease first, followed by a gradual increase with speed. The curve under 500 N exhibits a high COF with all speeds. As the load increases, the COF pattern remains largely consistent with speeds that are less than 1500 rpm. The COF for the curve under 800 N has a steady and linear increase beyond 1500 rpm, while that under 1100 N gradually increases after 3500 rpm. In contrast, the COF values under 1500 N are relatively stable at 0.05 after 1500 rpm. However, the COF of all four curves in 90 °C water is lower than that in 25 °C water under the same loads. The difference in the COF decreases with an increase in the load to 1500 N with a similar trend for speed. Note that the curve pattern under 1100 N in 90 °C (5 MPa) water differs significantly from that of the 25 °C (1 MPa) curve. The COF of the 90 °C curve decreases and then increases with speed, and there is an obvious turning point at 1000 rpm. The COF of the 25 °C curve first rapidly decreases with speed up to 1000 rpm and then hardly changes. Differently in the 25 °C water, the COF of 800 N and 1100 N in 90 °C water with 500–3500 rpm is lower than that of 1500 N. The transition in lubrication regimes may be carried out due to differences in the water environments.

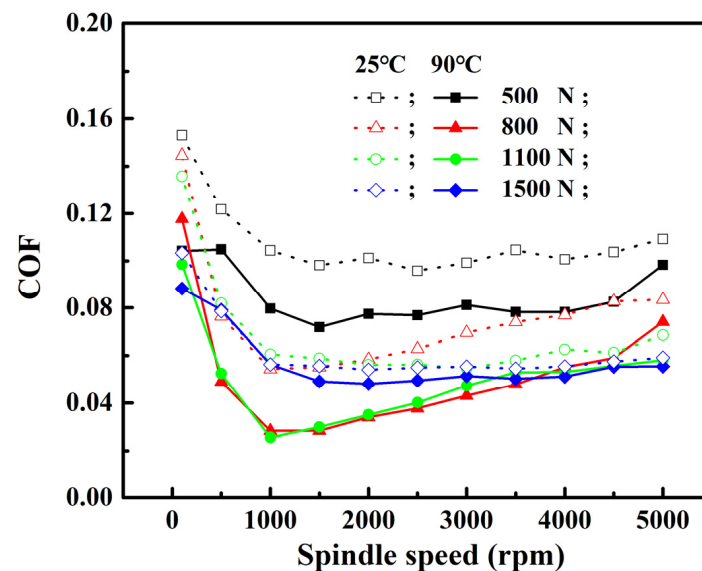


Figure 6. Stribeck curves of the siliconized graphite rings manifest as COF as a function of the step-down spindle speeds from 5000 rpm to 100 rpm under the applied loads of 500–1500 N in 25 °C (1 MPa) and 90 °C (5 MPa) water, respectively.

3.3. Wear Tests in 25 °C (1 MPa) and 90 °C (5 MPa) Water Environments

Figure 7 shows the COF of siliconized graphite rings as a function of the duration of 7200 s under the selected applied loads of 500–1500 N with spindle speeds of 100–5000 rpm in 25 °C (1 MPa) and 90 °C (5 MPa) water, respectively. For the COF in 25 °C water, there is a running-in process in the initial stage under the lower and higher loads of 500 and 1500 N with 100 rpm, and it then remains stable. The COF change shows typical fluctuation, and the fluctuation amplitude under 500 N is smaller than that under 1500 N. However, a smaller COF of 0.085 with smoother variation exists under 1500 N. As the speed increases to 1000 rpm and 2000 rpm, there is always a tendency toward running-in and then oscillating with regularity. A significant decrease in the average COF value is obtained at 0.04. Nevertheless, this magnitude is considerably less than that of 100 rpm. As the speed increases to 5000 rpm, no running-in process under 500 N and 800 N is detected, and the COF oscillates irregularly within a slightly larger magnitude. The average COF value under 800 N with 5000 rpm is 0.08, which is less than that observed under 500 N with 5000 rpm. The COF change obviously depends on the speed. For all the wear tests in 90 °C water, the COF measured is lower than that in 25 °C water. With 100 rpm, the

COF under 500 N and 1500 N shows regular fluctuations. The amplitudes under 500 N are smaller than those under 1500 N. For both curves in 90 °C and 25 °C water, the initial COF in 90 °C water is higher than that in 25 °C, because the stable COF achieved later is basically consistent with that in 90 °C. The average COF under 1500 N is smaller than that under 500 N. As the speed increases to 1000–2000 rpm, a longer running-in process occurs under 800 N. Furthermore, the average COF value of 0.015 in 90 °C water is much lower than that in 25 °C water. Note that the COF patterns under 1100 N are significantly different in 25 °C (1 MPa) and 90 °C (5 MPa) water environments, while the COF with 2000 rpm in 90 °C water is more closely aligned that with 5000 rpm. With a speed of 5000 rpm, the COF in both water environments are similar to the average values in oscillation patterns.

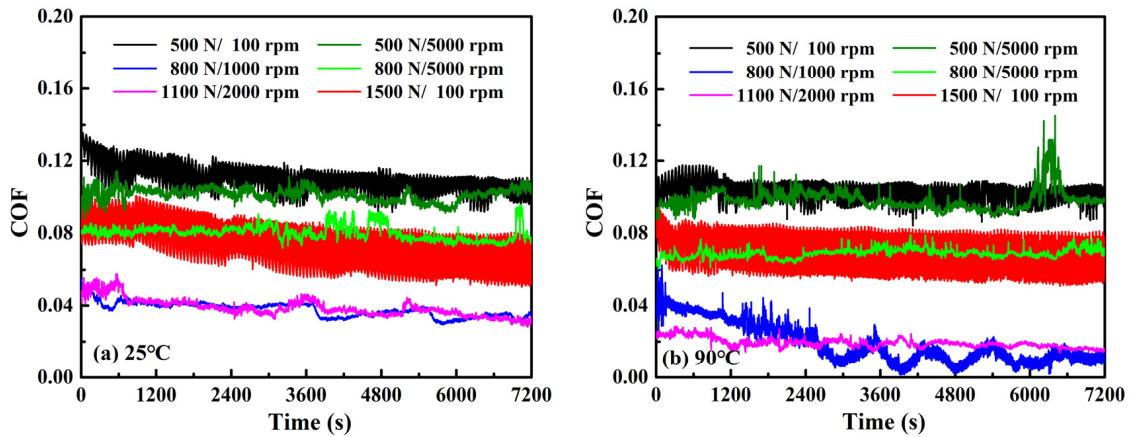


Figure 7. COF of the siliconized graphite rings as a function of the duration of 7200 s under the selected applied loads of 500–1500 N with spindle speeds of 100–5000 rpm in (a) 25 °C (1 MPa) and (b) 90 °C (5 MPa) water environments, respectively.

Figure 8 shows the worn surface roughness R_a of siliconized graphite rings under the applied loads of 500–1500 N with spindle speeds of 100–5000 rpm in 25 °C and 90 °C water environments, respectively. The original ring has a surface roughness R_a of 0.028 μm . For all each R_a of siliconized graphite in 25 °C water, the minimal R_a of 0.015 μm is detected under 1500 N with 100 rpm. A maximal R_a of 0.026 μm is obtained with 5000 rpm under 800 N. The R_a change in 90 °C water is similar to that in 25 °C water, but each R_a in 90 °C water is less than or equal to that under the same conditions in 25 °C water. It is larger with 5000 rpm under 500 and 800 N, which is close to the original.

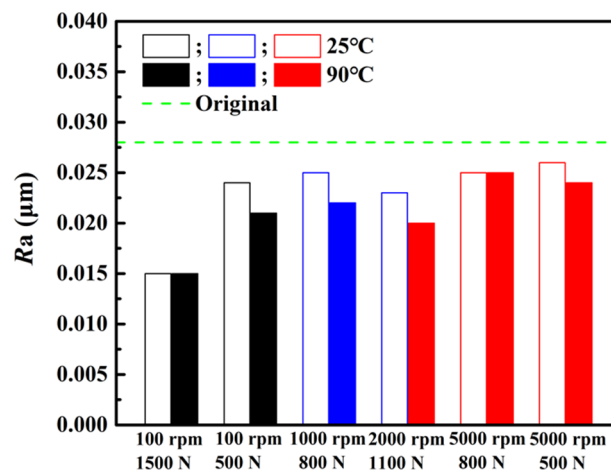


Figure 8. Surface roughness R_a of the siliconized graphite rings under the applied loads of 500–1500 N with spindle speeds of 100–5000 rpm in 25 °C (1 MPa) and 90 °C (5 MPa) water environments, respectively.

Figure 9 shows the wear depths of siliconized graphite rings for 7200 s duration under the applied loads of 500–1500 N with a spindle speed of 100–5000 rpm in 25 °C and 90 °C water environments, respectively. In general, the wear depth is more sensitive to the spindle speed, as it significantly decreases from 100 to 5000 rpm, in spite of some effects of loads with the lower speed of 100 rpm. Specifically, a maximal wear depth of 0.97 μm is obtained under 1500 N with 100 rpm in 25 °C water. It decreases to 0.65 μm under 500 N with 100 rpm. When the speed increases to 1000 and 2000 rpm under 800 and 1100 N, the wear depth decreases to 0.25 and 0.22 μm, respectively. At 5000 rpm under 500 and 800 N, the wear depth decreases to 0.11–0.14 μm with a lower wear loss, and the effect of the load is limited with higher speed. Similarly, the change in wear depths in 90 °C water is basically consistent with that in 25 °C water, whereas it is slightly higher in 90 °C water except under 1100 N with 2000 rpm. The maximal wear depth of 0.97 μm is identical with 100 rpm under 1500 N in both water environments. The wear depth is 0.71 μm under 500 N with 100 rpm, which is higher by 0.06 μm in 90 °C water. This suggests that water environments have a major influence on the wear behavior with a lower speed of 100 rpm under 500 N, and the influence gradually diminishes or disappears as the load increases to 1500 N. The wear depth is 0.32 μm under 800 N with 1000 rpm in 90 °C water, which is higher by 0.07 μm than that in 25 °C water. However, it is 0.18 μm under 1100 N with 2000 rpm in 90 °C water and lower than that of 0.22 μm in 25 °C water. There is little difference under 500 and 800 N with 5000 rpm in both water environments. The wear depth is between 0.11 and 0.15 μm: there is virtually no wear. Nevertheless, the wear depth in 90 °C water is still 0.01 μm greater than that in 25 °C under the same conditions of 500 and 800 N with 5000 rpm, respectively.

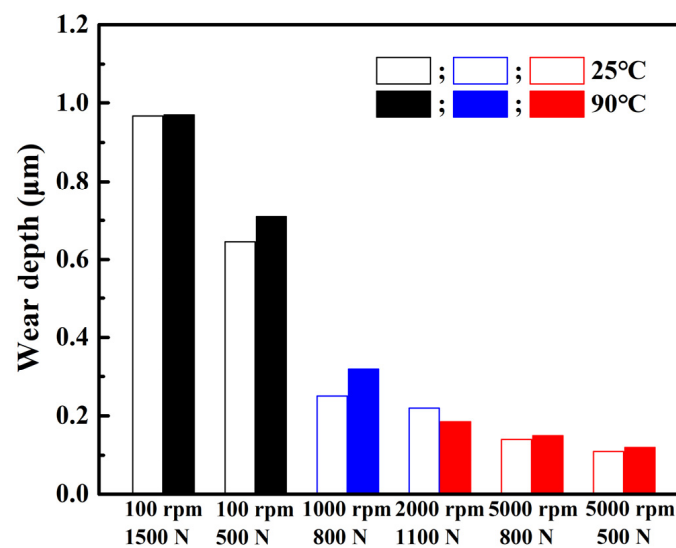


Figure 9. Wear depths of the siliconized graphite rings for 7200 s duration under the applied loads of 500–1500 N with a spindle speed of 100–5000 rpm in 25 °C (1 MPa) and 90 °C (5 MPa) water environments, respectively.

Figure 10 shows the residual stresses of the graphite, Si, and SiC phases on the worn surface of siliconized graphite rings under the applied loads of 500–1500 N with spindle speeds of 100–5000 rpm in 25 °C and 90 °C water, respectively. Residual compressive stress presents itself on the original surfaces of all the C, Si, and SiC phases, which is consistent with that by grinding [26]. The residual stress of C on the worn surface under all conditions is similar to that of the original with an average value of around −4 MPa. For the original siliconized graphite rings, Si has a residual stress of −33.1 MPa and SiC of −49.2 MPa. Considering that SiC accounts for nearly 60% of the overall volume, the findings predominantly outline the stresses in SiC. For the stress in 25 °C water, it increases from −55.2 MPa under 500 N to −70.4 MPa under 1500 N with 100 rpm. Alongside the speed from 100 to

1000–2000 rpm, the residual stress increases by only -70.4 to -80 MPa. However, as the speed reaches 5000 rpm under 500 and 800 N, the residual stress substantially increases to -133 MPa. In 90°C water, the surface stress of -60.4 MPa is larger than that of -55.2 MPa in 25°C water under 500 N with 100 rpm. The residual stress of -81.5 MPa under 800 N with 1000 rpm is larger than that of -72.2 MPa in 25°C water. Additionally, the residual stress of 800 N is comparable to that of 1100 N in 25°C water, but smaller than that of 1100 N in 90°C water. In contrast, the stress with 5000 rpm displays an opposing trend, which is larger under both 500 N and 800 N in 25°C water than that in 90°C water.

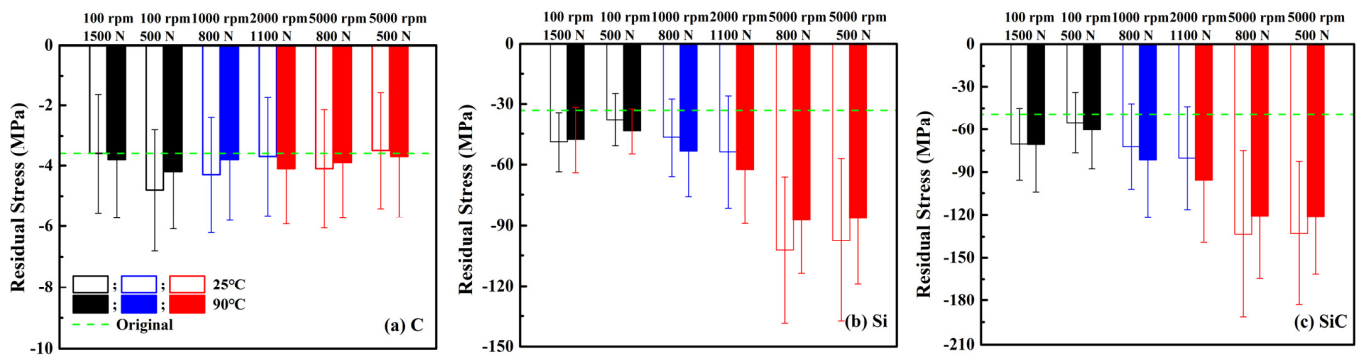


Figure 10. Residual stresses of (a) C, (b) Si, and (c) SiC phases on the worn siliconized graphite rings under the applied loads of 500–1500 N with spindle speeds of 100–5000 rpm in 25°C (1 MPa) and 90°C (5 MPa) water environments, respectively.

Figure 11 shows the SEM images of the worn surface morphology of siliconized graphite rings under the applied loads of 500–1500 N with spindle speeds of 100–5000 rpm in 25°C (1 MPa) water environments. Three distinct regions of grayscale are observed as the C, Si, and SiC phases, for the original siliconized graphite ring according to the composition of the siliconized graphite (Figure 11a). The surface morphology of the SiC phase under high-magnification SEM is further imaged, as in the area with the blue frame in Figure 11a (Figure 11b). The porous microstructure of SiC is observed on the surface with most of the pores being micrometer-scale in width. The maximal diameter of pores exceeds $2\ \mu\text{m}$. The red arrow points to the sliding direction (Figure 11c–h). Some ploughs along with the sliding direction are observed on the C and Si phases and the porous feature on the original SiC phase is partially maintained on the SiC phase under 500 N with 100 rpm (Figure 11c). The pores are mostly covered or filled in by wear debris, leading to decreasing number of pores compared with the original SiC. For the surface morphology under 1500 N with 100 rpm, the entire surfaces are flat with few pores overall, as if it has been polished (Figure 11d). A few distinct ploughs are observed under 800 N with 1000 rpm. There are two types of ploughs: those that pass through all the C, Si, and SiC phases, and those that pass through only the C and Si phases (Figure 11e). Obviously, the ploughs that pass through all the phases are a result of SiC asperities due to its higher hardness, while the other ploughs that pass through only the C and Si phases are also attributed to the Si asperities. Therefore, the ploughs on the SiC phase are fewer and shallower compared to those on the C and Si phases. Unlike the worn surface under 500 and 1500 N with 100 rpm, the surface morphology under 800 with 1000 rpm retains nearly all the features of the original surface except for the obvious ploughs caused by wear debris. The surface morphology under 1100 N with 2000 rpm is similar to that under 800 N with 1000 rpm (Figure 11f). The ploughs are also divided into two types, albeit with a slightly smaller plough density. The worn surfaces are similar to those with 5000 rpm under 500 and 800 N, with no significant change on the C phase (Figure 11g,h), while a wavy surface appears on the SiC phase. Moreover, there are several uniformly flow-oriented striae on the Si phase, which are sparse under 500 and 800 N with 5000 rpm.

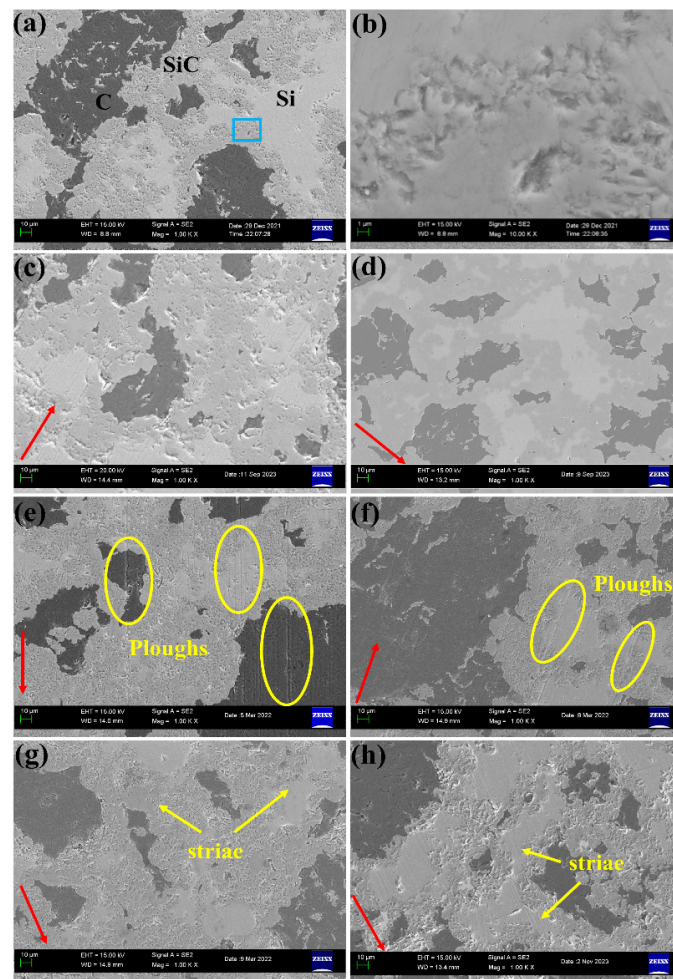


Figure 11. SEM images of the worn surface morphology of siliconized graphite rings under the applied loads of 500–1500 N with spindle speeds of 100–5000 rpm in 25 °C (1 MPa) water environments. (a) Original; (b) enlargement of SiC phase from the blue frame in (a); (c) 500 N/100 rpm; (d) 1500 N/100 rpm; (e) 800 N/1000 rpm; (f) 1100 N/2000 rpm; (g) 500 N/5000 rpm; and (h) 800 N/5000 rpm.

Figure 12 shows the SEM images of the worn surface morphology of siliconized graphite rings under the applied loads of 500–1500 N with spindle speeds of 100–5000 rpm in a 90 °C (5 MPa) water environment. There are also a few ploughs on the C and Si phase under 500 N with 100 rpm [Figure 12a], which are fewer compared to those under 500 N with 100 rpm in 25 °C water. The majority of the pores on the SiC surfaces are no longer observable with only few remaining, resulting in a relatively flat surface overall, suggesting that the worn surfaces experience varying wear degrees under 500 N with 100 rpm in both water environments. In contrast, the worn surfaces are consistent under 1500 N with 100 rpm in both water environments. Compared to the surface under 800 N with 1000 rpm in 25 °C water, the ploughs on the surface are minimal with only slight traces on C and Si in 90 °C water (Figure 12c). The porous features of the SiC surface are basically similar to those of the original. Moreover, the surface under 1100 N with 2000 rpm is almost indistinguishable from that of the original, with no visible indications of wear present (Figure 12d). All worn surfaces with 5000 rpm under 500 and 800 N in both water environments show similar features. In general, no significant change is observed on the C phase, whereas the wavy surface that appeared on the SiC phase varies in extent visually under 500 and 800 N. Markedly, numerous uniformly flow-oriented striae appear on the Si phase, which remain sparse under 500 and 800 N with 5000 rpm in 25 °C water, but they

become prominent and dense under 500 and 800 N with 5000 rpm in 90 °C water. The stria density on the Si phase is larger under 800 N with 5000 rpm. High-magnification images of the big and small blue frames in Figure 12f are shown in Figure 12g and h, respectively. After a 7200 s duration under 800 N with 5000 in 90 °C water, the worn surface of the SiC phase exhibits visible cracking (Figure 12g), initiating from a small pore and subsequently propagating downwards, resulting in a lot of forking. This cracking is absent on the other three worn surfaces with 5000 rpm under 500 and 800 N, suggesting that the worn surface is impacted by water temperature, pressure, and load simultaneously. On the other hand, the striae on the Si phase are perfectly aligned with the direction of wear (Figure 12h), appearing straight and densely packed. As there is no contact between the surfaces, it is likely that these striae form due to water film scouring.

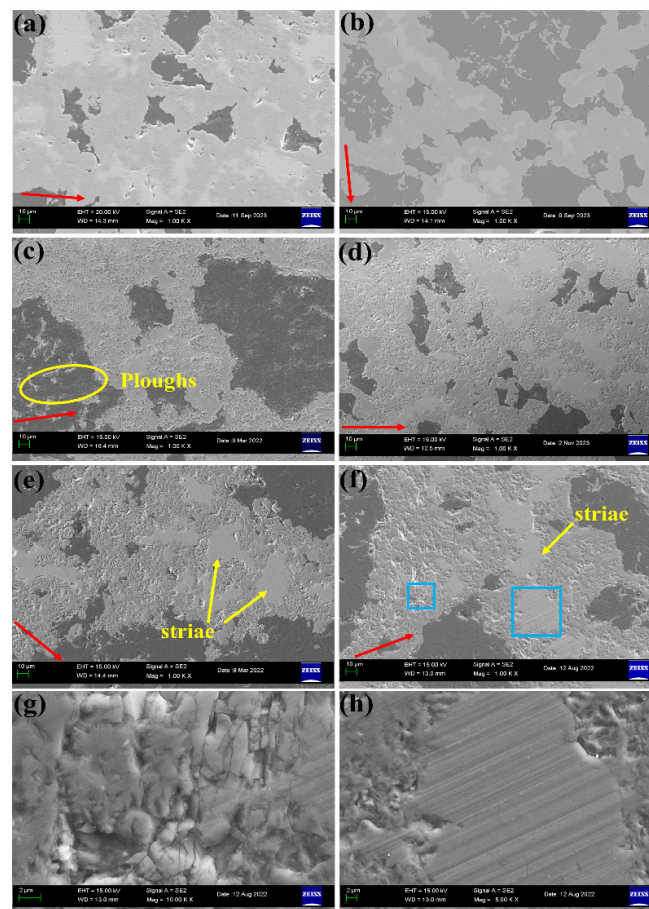


Figure 12. SEM images of surface morphology of siliconized graphite rings under the applied loads of 500–1500 N with spindle speeds of 100–5000 rpm in 90 °C (5 MPa) water environments as follows: (a) 500 N/100 rpm; (b) 1500 N/100 rpm; (c) 800 N/1000 rpm; (d) 1100 N/2000 rpm; (e) 500 N/5000 rpm; (f) 800 N/5000 rpm; and (g) and (h) show the enlargement of the area by the small and big blue frame in (f), respectively.

4. Discussion

4.1. Lubrication Regimes in High-Temperature and High-Pressure Water

Figure 13 shows the schematic diagrams of the lubrication regimes of siliconized graphite in 25 °C (1 MPa) and 90 °C (5 MPa) water environments, respectively. The lubrication regimes of siliconized graphite are distinguished not only by the Stribeck curves, but also by the worn surface morphology, wear depth, surface roughness, and residual stress during long-term wear tests. In 25 °C water, the boundary lubrication is a low-speed region less than 500 rpm under all the applied loads of 500–1500 N. The low-speed region

is more sensitive to loading, as it gradually expands with the load from 500 to 1500 N. The surface asperities between the specimen ring pairs are in direct contact and wear [27]. With loading, the surface contact becomes closer, the indentation depth greater, and wear more severe. The average COF values are close to or even exceed 0.1, which are manifested by the large fluctuation caused by the constant wear between siliconized graphite rings. The amplitude gradually increases, reaching a maximum of 0.045 under 1500 N. The worn surfaces of the C, Si, and SiC phases are similarly smooth with $R_a = 0.015 \mu\text{m}$, and the porous characteristics of original SiC mostly disappear as if it has been filled in and then polished. The larger wear depth of $0.65\text{--}0.97 \mu\text{m}$ indicates that the main wear mechanism of siliconized graphite under the boundary lubrication is abrasive wear caused by SiC and Si asperities, because, with regard to SiC and Si, the harder phase plays a crucial role relative to the wear depth under solid direct wear conditions. These asperities between surfaces are gradually smoothed out under 1500 N with 100 rpm, resulting in a reduced COF value of 0.8. The graphite particles disperse on the surface acting as a solid lubricant, which can stabilize wear after a stable friction film has formed on the worn surface [28]. However, the Si dispersed on the surface has a limited role in the abrasive wear [18]. The structural characteristics of SiC as the bone along with the self-lubricating graphite particles dispersed on the surface [29] ensure that the siliconized graphite maintains a relatively low wear depth of $0.97 \mu\text{m}$ compared to that of the other bearing materials [10–13]. The load is insufficient to completely smooth all the rough asperities within a 7200 s duration under 500 N with 100 rpm, which results in some wear ploughs on the surface, and the wear depth decreases to $0.65 \mu\text{m}$, suggesting that the siliconized graphite is currently under boundary lubrication but is transitioning towards mixed lubrication with limited lubrication from water, and the loading is mainly sustained in direct contact.

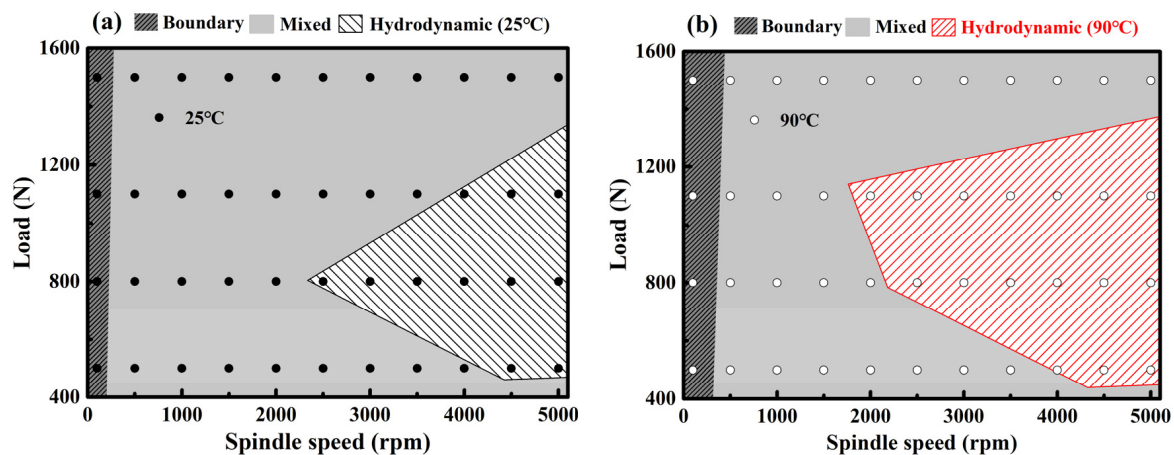


Figure 13. Schematic diagrams of the lubrication regimes of siliconized graphite rings under the applied loads of 500–1500 N with spindle speeds of 100–5000 rpm in 25 °C (1 MPa) (a) and 90 °C (5 MPa) (b) water environments, respectively.

The mixed lubrication is obtained under a combination of 500–1500 N and 500–5000 rpm conditions in 25 °C water, with different critical speeds corresponding to each load. It is a transition region from the boundary to hydrodynamic lubrication and the load is supported by both water film and solid contact [30]. The average COF value is 0.04 under both the conditions of 800 N with 1000 rpm and 1100 N with 2000 rpm, and the changes in the COF are displayed by a running-in process due to surface asperities at the beginning of wear, followed by a stabilized state of regular fluctuation with smaller amplitude. There is minimal change in the worn surface morphology of each phase with $R_a = 0.023 \mu\text{m}$, which is mainly reflected in the ploughs on the surface. The ploughs that pass through all the phases are a result of SiC due to its higher hardness, while the other ploughs that only pass through the C and Si phases are attributed to the SiC and Si asperities. In the mixed lubrication state where both water film and solid contact coexist, the solid contact is randomized

between surface asperities. Both SiC and Si, which are relatively hard, scratch the surfaces. The residual stress change in SiC and Si is completely consistent, indicating that their tribological properties and functions are similar during wear. The proportion of the load carried by the water film and solid varies under different loads with varying speeds [31]. A thicker water film under 1100 N with 2000 rpm compared to a lower speed of 1000 rpm results in a shallower indentation depth of the rough surface, as well as lighter scratches on the worn surface with fewer ploughs. Although the lubrication provided by water is greater than that of the graphite particles on the worn surface of siliconized graphite, the smaller wear depth of 0.23–0.25 μm is obtained under the combined lubrication of the water and the graphite particles on the siliconized graphite.

The hydrodynamic lubrication is a high-speed region of 2500–5000 rpm under 500–1100 N in 25 °C water, indicating that it is generally easier to achieve with higher speeds. This region exhibits a typical form of a C-curve, with a certain correlation between speeds and loads. The intermediate inflection point is 800 N with 2500 rpm, representing the minimal speed required to achieve hydrodynamics in 25 °C water. The critical speeds under 500 N and 1100 N are 4500 and 4000 rpm, respectively, suggesting that the higher speeds result in the lower effect of the load. Accordingly, the ring pairs are completely separated by a full water film, leading to no wear behavior between the solids [32]. Therefore, although the COF value is the same at 0.1, there is not a solid running-in process, and it fluctuates randomly around an average value throughout. The graphite on the worn surface does not change, whereas SiC exhibits a wavy feature on the surface caused by a tribochemical reaction with water [33,34] and even cracking under the action of oxide stress. The Si surface displays numerous uniformly flow-oriented striae. The density of the striae is very large, which is different from that of the regular solid wear trace. The striae are scoured by the water film over a long time due to viscous shear forces. The residual compressive stress in Si increases due to the water film, whereas in SiC it is a result of both the water film and tribochemical reactions. The wear depth is less than 0.14 μm under 500 and 800 N with 5000 rpm, reflecting the consumption of SiC by the shedding of SiO_2 generated by the reaction between SiC and water [33,34].

In 90 °C water, the boundary lubrication region expands when the speed is less than 500 rpm under 500–1500 N, because the viscosity of the water is 2.74×10^{-4} Pa·s, which is an order of magnitude lower than the 1.1×10^{-3} Pa·s in 25 °C (1 MPa) water. The average COF and fluctuation amplitude are similar to those obtained in 25 °C water. The worn surface is smooth and the wear depth under 1500 N with 100 rpm is completely consistent in both water environments, suggesting that the influence of the viscosity change in water is limited under higher loads. However, the wear depth under 500 N with 100 rpm is 0.71 μm , which is deeper than that obtained under the same condition in 25 °C water. The expansion of the boundary lubrication region is directly caused by the decrease in water viscosity, leading to transition delay to the mixed lubrication. Furthermore, the limited lubrication of water deteriorates under 500 N with 100 rpm in 90 °C water. Mixed lubrication occurs under a combination of 500–1500 N and 500–5000 rpm conditions in 90 °C water, with the corresponding critical speed varying under each load. However, the region is significantly reduced to 1500 rpm under 1100 N. The average COF value is reduced to 0.02, with the smaller one of 0.005 under 800 N with 1000 rpm. The worn surface is reflected in surface ploughing, while the density of ploughs is lower with $R_a = 0.022$ μm , compared to that of those in 25 °C water. This is due to an increase in water film thickness and a decrease in solid contact. The wear depth of 0.32 μm is slightly higher than that of 0.25 μm under 800 N with 1000 rpm in 25 °C water, due to the longer running-in process. Hydrodynamic lubrication occurs at high speeds of 2000–5000 rpm under 500–1100 N in 90 °C water, taking the similar form of a C-curve. The region expands in both directions of the load increase and speed decrease. The minimal speed of hydrodynamics decreases to 2000 rpm under 1100 N, and it also slightly decreases under 500 N and 800 N. The average COF value decreased to 0.08 due to viscosity, but the fluctuation amplitude is almost same under 5000 rpm. The worn surface is mainly reflected in the larger wavy feature of SiC, indicating

that the SiC phase is more likely to react in high-temperature and high-pressure water [35], while the wear depth is slightly increased to 0.15 μm and more SiC is consumed under the same conditions.

4.2. Integrated Evaluation by G Duty Parameters

The lubrication regime transitions are distinguished when the COF is plotted versus a G duty parameter, which is expressed [36] as follows:

$$G = \frac{\mu V \Delta r}{F} \quad (1)$$

where μ is the viscosity of the liquid, V the sliding speed, Δr the friction surface width, and F the applied load. In order to establish the dependence of the tribological properties on the operating conditions, Figure 14 shows the wear depths of the siliconized graphite rings under the applied loads of 500–1500 N with spindle speeds of 100–5000 rpm in 25 °C (1 MPa) and 90 °C (5 MPa) water, as a function of the G duty parameter. Based on the wear depth obtained in the continuous wear tests of a 7200 s duration, a relationship between wear depth and logarithm of G values is summarized.

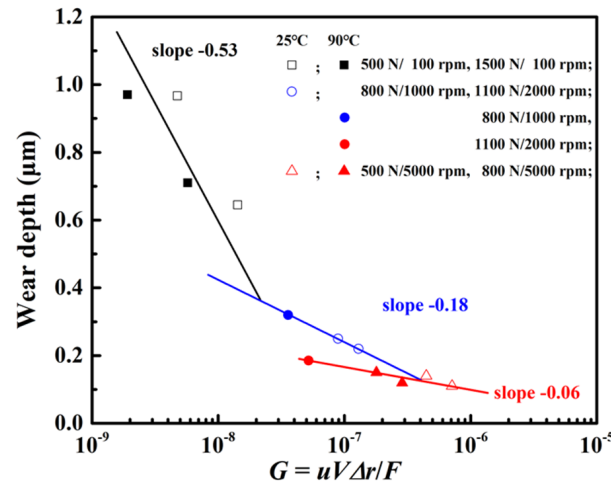


Figure 14. Wear depths of the siliconized graphite rings under the applied loads of 500–1500 N with spindle speeds of 100–5000 rpm in 25 °C (1 MPa) and 90 °C (5 MPa) water environments, as a function of G duty parameter.

This can be divided into three linear segments with different slopes relative to the varying G values. The black segment with a slope of -0.53 contributes to the boundary lubrication and is characterized by wear depth under 500 N and 1500 N with the same 100 rpm in both water environments. The wear depth linearly decreases with the G values. The worn surface has the low roughness R_a of about 0.015 μm . The worn surface exhibits typical abrasive wear from SiC and Si asperities. Meanwhile, the COF pattern manifests in stable fluctuation with a larger magnitude due to constant contact between the ring pairs. The blue segment with a slope of -0.18 is attributed to the mixed lubrication. The wear depths gradually decrease with the G values. The worn surface roughness R_a is between 0.022 and 0.025 μm . The worn surface has typical surface ploughing from SiC and Si asperities, because the density of the ploughs decreases with the proportion of the load carried by the full water film. The COF changes correspond to the running-in process due to surface asperities at the beginning of wear, followed by a stabilized state of smaller fluctuation amplitude. The red segment with a slope of -0.06 deserves to characterize the hydrodynamic lubrication by the lower wear depth under 500 and 800 N with the same 5000 rpm in both water environments. The wear depths marginally decrease with the G values. The worn surface roughness is more similar to that of the original siliconized graphite. There is no apparent change in graphite on the worn surface, while the wavy

feature of SiC and uniform flow-oriented striae of Si contribute to the hydrodynamic lubrication. The surface morphology is caused by the water film scouring the worn surface. The COF fluctuates randomly around an average value throughout. Note that the wear depth of 0.18 μm obtained under 1100 N with 2000 rpm in 90 °C water in the slope of -0.06 indicates that the lubricated regimes of siliconized graphite are not unique at a G value. Since the lubrication regime is a non-transient transition from the boundary, mixed, to hydrodynamic lubrications, it is possible to correspond simultaneously to boundary and mixed lubrications or mixed and hydrodynamic lubrications within a certain interval of the same G determined by different temperature, pressure, loads, and speeds [16–18]. And the exact lubrication regime is figured out by means of sloping segments. The integrated evaluation method manifested as the slope of the wear depths versus the logarithm of G values is used to identify the lubrication regimes from boundary, mixed, to hydrodynamic lubrications for the water-lubricated thrust bearings of the main coolant pump in a nuclear power plant.

5. Conclusions

- (1) The effect of the microstructure of siliconized graphite on the tribological properties is investigated by Stribeck curves and wear tests under an applied load of 500–1500 N with a spindle speed of 100–5000 rpm in both 25 °C (1 MPa) and 90 °C (5 MPa) water environments, respectively.
- (2) The lubrication regimes of self-mated siliconized graphite on a ring-on-ring configuration are characterized by the coefficient of friction, wear depth, and worn morphology with surface roughness and residual stress, which are dependent not only on the applied load and spindle speed but also on the graphite, Si, and SiC phases of siliconized graphite.
- (3) The abrasive wear of SiC and Si asperities together with graphite solid lubrication is attributed to the boundary lubrication. The partially abrasive wear in the thin water film causes the mixed lubrication. The full water film scouring with the wavy feature of SiC and uniform flow-oriented striae of Si contributes to the hydrodynamic lubrication.
- (4) An integrated evaluation method of the G duty parameters as a function of the wear depths with the segment slopes is successfully used to identify the lubrication regimes from boundary, mixed, to hydrodynamic lubrications for the water-lubricated thrust bearings of the main coolant pump in a nuclear power plant.

Author Contributions: Conceptualization, S.L. and B.Z.; Methodology, S.L., B.Z. and T.L.; Investigation, S.L. and T.L.; Resources, L.C. and W.W.; Data curation, S.L.; Writing—original draft, S.L.; Writing—review & editing, M.L.; Project administration, M.L. All authors have read and agreed to the published version of the manuscript.

Funding: This research was funded by the National Natural Science Foundation of China (NSFC) under Grant No. U21B2078, and the National Key Research and Develop Program of China under Grant No. 2023YFB3408102.

Data Availability Statement: The data presented in this study are available on request from the corresponding author. The data are not publicly available due to privacy or ethical restrictions.

Conflicts of Interest: Authors Baojun Zhang, Long Cai and Weiguang Wang were employed by the company Sino Seal Holding Co., Ltd., Harbin Electric Power Equipment Co., Ltd. The remaining authors declare that the research was conducted in the absence of any commercial or financial relationships that could be construed as a potential conflict of interest.

References

1. Baumgarten, S.; Brecht, B.; Bruhns, U.; Fehring, P. Reactor Coolant Pump Type RUV for Westinghouse Electric Company LLC Reactor AP1000TM. In Proceedings of the International Congress on Advances in Nuclear Power Plants, San Diego, CA, USA, 13–17 June 2010; pp. 177–185.
2. Li, T.; Ma, L. Research and Development of Wet Winding Motor Reactor Coolant Pump for Generation 3 Nuclear Power Plant. In Proceedings of the ASME Proceedings of 29th International Conference on Nuclear Engineering, Online, 8–12 August 2022.

3. Barbosa, J.; Cavallini, A.A., Jr.; Santos, I.; Steffen, V., Jr. Dynamic Behavior of A Tilting-Pad Thrust Bearing Operating under a Hybrid Lubrication Regime. *ASME J. Tribol.* **2023**, *145*, 114101. [[CrossRef](#)]
4. Yu, X.; Tang, B.; Wang, S.; Han, Z.; Li, S.; Chen, M.; Zhang, R.; Wang, J.; Jiao, J.; Jiang, H. High-speed and heavy-load tribological properties of Hydrostatic Thrust Bearing with Double Rectangular Recess. *Int. J. Hydrogen Energy* **2022**, *47*, 21273–21286. [[CrossRef](#)]
5. Huang, J.; Zhou, X.; Wang, J.; Tang, X.; Kuang, F. Influence of Temperature on Friction of Polymeric Materials in Water. *Wear* **2019**, *426*, 868–876. [[CrossRef](#)]
6. Kitaoka, S.; Tsuji, T.; Katoh, T.; Yamaguchi, Y.; Kashiwagi, K. Tribological Characteristics of SiC Ceramics in High-Temperature and High-Pressure Water. *J. Am. Ceram. Soc.* **1994**, *77*, 1851–1856. [[CrossRef](#)]
7. Yin, T.; Wei, D.; Wang, T.; Xie, Z. Thermal Compression and Accumulation Effect on Lubrication Regime Transition Mechanism of Water Seal. *Tribol. Int.* **2023**, *181*, 108285. [[CrossRef](#)]
8. Wolf, R. Boronized and Siliconized Graphites-Material Processing and Effects on Properties. *J. Nucl. Mater.* **1994**, *212*, 1174–1177. [[CrossRef](#)]
9. Krasilnikov, A.; Ryaposov, A. Corrosion Resistance of Siliconized Graphite Based Structural Materials under Decontamination Conditions. *At. Energy* **2022**, *132*, 258–261. [[CrossRef](#)]
10. Yu, P.; Li, G.; Zhang, L.; Zhao, F.; Chen, S.; Dmitriev, A.; Zhang, G. Regulating Microstructures of Interpenetrating Polyurethane-Epoxy Networks towards High-Performance Water-Lubricated Bearing Materials. *Tribol. Int.* **2019**, *131*, 454–464. [[CrossRef](#)]
11. Liang, X.; Yang, Z. Experimental Study on the Influence of Friction Pair Material Hardness on the Tribological Behaviors of Water Lubricated Thrust Bearings. *Ind. Lubr. Tribol.* **2021**, *73*, 929–936. [[CrossRef](#)]
12. Yu, H.; Zheng, W.; Zhang, C.; Chen, S.; Tian, G.; Wang, T. Dual Network Co-Crosslinked HNBR Composites with Enhanced Tribological Properties under Water Lubrication. *Lubricants* **2024**, *11*, 534. [[CrossRef](#)]
13. Wodtke, M.; Wasilczuk, M. Evaluation of Apparent Young's Modulus of the Composite Polymer Layers Used as Sliding Surfaces in Hydrodynamic Thrust Bearings. *Tribol. Int.* **2016**, *97*, 244–252. [[CrossRef](#)]
14. Hyuga, H.; Yoshizawa, I.; Hirao, K.; Rani, D.; Jones, M. Tribological Behavior of Si₃N₄ and Si₃N₄/carbon Fiber Composites Against Stainless Steel under Water Lubrication for a Thrust-Bearing Application. *Int. J. Appl. Ceram. Technol.* **2008**, *5*, 111–118. [[CrossRef](#)]
15. Liang, Y.; Wang, W.; Zhang, Z.; Xing, H.; Wang, C.; Zhang, Z.; Gao, D. Effect of Material Selection and Surface Texture on Tribological Properties of Key Friction Pairs in Water Hydraulic Axial Piston Pumps: A Review. *Lubricants* **2023**, *11*, 324. [[CrossRef](#)]
16. Xia, H.; Wang, J.; Shi, Z.; Qiao, G. Reciprocating Friction and Wear Properties of Mesocarbon Microbeads-Based Graphite and Siliconized Graphite. *J. Nucl. Mater.* **2013**, *433*, 341–344. [[CrossRef](#)]
17. Xue, Z.; Xue, R.; Zhang, N.; Zhang, L.; Liu, X.; Hou, B.; Zhang, Y.; Wang, J. Water-lubricated Friction Properties of C/C-SiC Composites with Different SiC-phase Contents Fabricated by RMI. *Tribol. Trans.* **2021**, *64*, 468–476. [[CrossRef](#)]
18. Li, Z.; Zhu, Z.; Yu, X.; Li, K.; Wang, Z.; Zhang, Z.; Wang, Y. Enhancement of Tribological Properties in Siliconized Graphite via Hierarchically Hybrid SiC/C Composite. *Prog. Nat. Sci. Mater. Int.* **2021**, *31*, 255–263. [[CrossRef](#)]
19. Yuan, Z.; He, Y.; Cheng, K.; Duan, Z.; Wang, L. Effect of self-developed graphene lubricant on tribological behaviour of silicon carbide/silicon nitride interface. *Ceram. Int.* **2019**, *45*, 10211–10222. [[CrossRef](#)]
20. Wan, F.; Pizada, T.; Liu, R.; Wang, Y.; Qi, G.; Zhang, C.; Marrow, T. Structure and Flexural Properties of 3D Needled Carbon Fiber Reinforced Carbon and Silicon Carbide (C/C-SiC) Composites Fabricated by Gaseous and Liquid Silicon Infiltration. *Ceram. Int.* **2019**, *45*, 17978–17986. [[CrossRef](#)]
21. Chae, S.; Choi, S.-H.; Kim, N.; Sung, J.; Cho, J. Integration of Graphite and Silicon Anodes for the Commercialization of High-Energy Lithium-Ion Batteries. *Angew. Chem. Int. Ed.* **2020**, *59*, 110–135. [[CrossRef](#)]
22. Tong, Y.; Wang, L.; Wang, B.; Hu, Y.; Cai, Z.; Ren, J.; Liu, J.; Li, S. Microstructure and Mechanical Behavior of Carbon Fiber Reinforced Carbon, Silicon Carbide, and Copper Alloy Hybrid Composite Fabricated by Cu-Si Alloy Melt Infiltration. *Adv. Compos. Hybrid Mater.* **2023**, *6*, 25. [[CrossRef](#)]
23. März, B.; Jolley, K.; Smith, R.; Wu, H. Near-surface Structure and Residual Stress in As-Machined Synthetic Graphite. *Mater. Des.* **2018**, *159*, 103–116. [[CrossRef](#)]
24. Fan, X.; Yin, X.; Cao, X.; Chen, L.; Cheng, L.; Zhang, L. Improvement of the Mechanical and Thermophysical Properties of C/SiC Composites Fabricated by Liquid Silicon Infiltration. *Compos. Sci. Technol.* **2015**, *115*, 21–27. [[CrossRef](#)]
25. Tong, Y.; Bai, S.; Liang, X.; Qin, Q.; Zhai, J. Reactive Melt Infiltration Fabrication of C/C-SiC Composite: Wetting and infiltration. *Ceram. Int.* **2016**, *42*, 17174–17178. [[CrossRef](#)]
26. Li, W.; Long, G.; Shi, F.; Zhou, S.; Yin, J.; Yang, J. Influence of the Fiber Orientation on 3D C/C-SiC Composite Material and its Formation Mechanism of the Machining Surface. *Int. J. Adv. Manuf. Technol.* **2022**, *118*, 2725–2743. [[CrossRef](#)]
27. Zhang, J.; Meng, Y. Boundary Lubrication by Adsorption Film. *Friction* **2015**, *3*, 115–147. [[CrossRef](#)]
28. Ahmad, I.; Anwar, S.; Xu, F.; Zhu, Y. Tribological Investigation of Multilayer Graphene Reinforced Alumina Ceramic Nanocomposites. *ASME J. Tribol.* **2019**, *141*, 022002. [[CrossRef](#)]
29. Calderon, N.; Martinez-Escandell, M.; Narciso, J.; Rodriguez-Reinoso, F. The Combined Effect of Porosity and Reactivity of the Carbon Preforms on the Properties of SiC Produced by Reactive Infiltration with Liquid Si. *Carbon* **2009**, *47*, 2200–2210. [[CrossRef](#)]
30. Azam, A.; Ghanbarzadeh, A.; Neville, A.; Morina, A.; Wilson, M.C.T. Modelling Tribochemistry in the Mixed Lubrication Regime. *Tribol. Int.* **2019**, *132*, 265–274. [[CrossRef](#)]

31. Hirani, H. *Fundamentals of Engineering Tribology with Application*; Cambridge University Press: Cambridge, UK, 2016.
32. Gropper, D.; Wang, L.; Harvey, T.J. Hydrodynamic Lubrication of Textured Surfaces: A Review of Modeling Techniques and Key Findings. *Tribol. Int.* **2016**, *94*, 509–529. [[CrossRef](#)]
33. Chen, M.; Kato, K.; Adachi, K. The Difference in Running-in Period and Friction Coefficient between Self-Mated Si₃N₄ and SiC under Water Lubrication. *Tribol. Lett.* **2001**, *11*, 23–28. [[CrossRef](#)]
34. Chen, M.; Kato, K.; Adachi, K. Friction and Wear of Self-mated SiC and Si₃N₄ Sliding in Water. *Wear* **2001**, *250*, 246–255. [[CrossRef](#)]
35. Zhang, W. Tribology of SiC Ceramics under Lubrication: Features, Developments, and Perspectives. *Curr. Opin. Solid State Mater. Sci.* **2022**, *26*, 101000. [[CrossRef](#)]
36. Brunetiere, N.; Francisco, A. Lubrication Mechanisms between Parallel Rough Surfaces. *Tribol. Lett.* **2019**, *67*, 116. [[CrossRef](#)]

Disclaimer/Publisher’s Note: The statements, opinions and data contained in all publications are solely those of the individual author(s) and contributor(s) and not of MDPI and/or the editor(s). MDPI and/or the editor(s) disclaim responsibility for any injury to people or property resulting from any ideas, methods, instructions or products referred to in the content.